Available online at www.sciencedirect.com
ScienceDirect
Cement and Concrete Research 37 (2007) 1096–1105
Cement and Concrete Research

Tensile and fiber dispersion performance of ECC (engineered cementitious composites) produced with ground granulated blast furnace slag

Jin-Keun Kim [a], Jeong-Su Kim [a], Gee Joo Ha [b], Yun Yong Kim [c,*]

[a] Department of Civil and Environmental Engineering, Korea Advanced Institute of Science and Technology (KAIST), 373-1, Guseong-dong, Yuseong-gu, Daejeon, 305-701, Korea
[b] Department of Architectural Engineering, Kyungil University, 33, Buho-ri, Hayang-up, Gyeongsan-si, Gyeongbuk, 712-702, Korea
[c] Department of Civil Engineering, Chungnam National University, 220, Gung-dong, Yuseong-gu, Daejeon, 305-764, Korea

Received 18 January 2007; accepted 19 April 2007

Abstract

An engineered cementitious composite (ECC) produced with ground granulated blast furnace slag was developed for the purpose of achieving moderately high composite strength while maintaining high ductility, represented by strain-hardening behavior in uniaxial tension. In the material development, single fiber pullout tests and matrix fracture tests were performed, followed by micromechanical analyses to properly select the range of mixture proportion. Subsequent direct tensile tests were employed to assess the strain-hardening behavior of the composite, which exhibited high ductility and strength with the addition of slag. High ductility is most likely due to enhanced workability and fiber dispersion performance which is attributed to the oxidized grain surface of slag, as verified by fiber dispersion tests. These results suggest that, within the limited slag dosage employed in the present study, the contribution of slag to fiber dispersion outweighs the side-effect of decreased potential for saturated multiple cracking, including a slight increase in matrix fracture toughness and fiber/matrix bond strength.
© 2007 Elsevier Ltd. All rights reserved.

Keywords: ECC; Ground granulated blast furnace slag; Micromechanics; Fiber dispersion; Tensile strain capacity

1. Introduction

In quasi-brittle cement-based materials such as concrete and mortar, fiber reinforcement is commonly used to improve the material's toughness and ductility [1]. Recently developed ultra-ductile engineered cementitious composites (ECCs) are an example of this approach [2,3]. ECC is a micromechanically designed cementitious composite that exhibits extreme tensile strain capacity (typically more than 2%) while requiring only a moderate amount of fiber. In this study, ground granulated blast furnace slag (slag hereafter) particles were employed to develop an ECC which exhibits moderately high composite strength while maintaining high ductility. Due to environmental and economical reasons, there is a growing trend to use industrial wastes or by-products as supplementary materials or admixtures in the production of composite cements. Slag is one such material that is being used in cement manufacturing as blast furnace slag cement. The surface action of slag has been discussed by various researchers [4]. It has been found that slag with a vitreous microstructure has not only a filling effect but also a dispersing effect associated with the surface chemical action [5].

To enhance the ductility of fiber reinforced cement-based materials, the properties of the matrix and the fiber/matrix interface are of primary concern for the overall behavior of the composite. In developing an ECC, it is more effective to utilize the properties of the matrix and the fiber/matrix interface. In the present study, various tests including fiber pullout and matrix fracture tests were performed on the composite and matrix with water–binder ratios (W/B) of 60%, 48%, 38%, 35%, and 28% to measure the fiber/matrix interfacial properties and the fracture toughness of the mortar matrix, respectively. A micromechanical analysis technique was employed using the obtained results in order to obtain the optimized mixture

* Corresponding author. Tel.: +82 42 821 7004; fax: +82 42 825 0318.
E-mail address: yunkim@cnu.ac.kr (Y.Y. Kim).

0008-8846/$ - see front matter © 2007 Elsevier Ltd. All rights reserved.
doi:10.1016/j.cemconres.2007.04.006

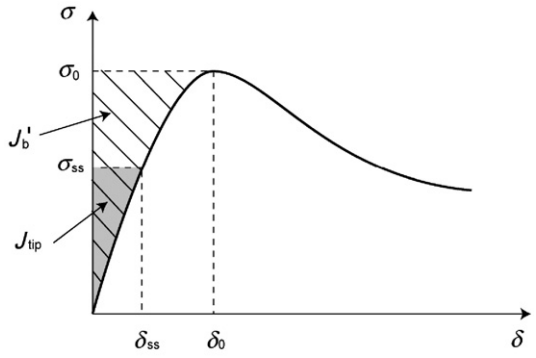

Fig. 1. A typical $\sigma(\delta)$ curve for a strain-hardening composite. The hatched area represents the complementary energy J_b' and the shaded area represents the crack tip toughness J_{tip}.

proportion for achieving strain-hardening behavior at a composite level. In addition to this process, SEM (scanning electron microscope) and fiber dispersion tests were performed to assess interfacial qualities and fiber dispersion performance. Subsequent uniaxial tensile tests were carried out to determine the strain-hardening behavior in uniaxial tension and to compare the tensile strain capacity between ECCs produced with slag (Slag-ECC hereafter) and those without slag.

Based on this mixture proportion prototype, diverse Slag-ECCs have been developed. Sprayable and self-consolidating versions of Slag-ECC have been developed by controlling the fluid properties in a fresh state. Details of this will be presented in a follow-up paper.

2. Design framework

2.1. Micromechanical design

The micromechanical design utilized herein mainly focuses on achieving strain-hardening in uniaxial tension, as the tensile ductility can be representative of the material ductility. A fundamental requirement for strain-hardening is the occurrence of steady state cracking. This requires that crack tip toughness J_{tip} be less than the complementary energy calculated from the bridging stress vs. crack opening curve, as illustrated in Fig. 1 [3],

$$J_{tip} \leq \sigma_0 \delta_0 - \int_0^{\delta_0} \sigma(\delta) \mathrm{d}\delta \equiv J_b' \tag{1}$$

$$J_{tip} = \frac{K_m^2}{E_c} \tag{2}$$

where σ_0 is the maximum bridging stress corresponding to the opening δ_0. K_m and E_c are the fracture composite elastic moduli. Eq. (1) is obtained by considering the balance of energy changes during the extension of a steady state flat crack. Another condition for strain-hardening is that the tensile first crack strength σ_{fc} must not exceed the maximum bridging stress σ_0,

$$\sigma_{fc} < \sigma_0 \tag{3}$$

where σ_{fc} is determined by the maximum preexisting flaw size a_0, and the matrix fracture toughness K_m. Satisfaction of Eqs. (1) and (3) is also necessary to achieve high ductile behavior, represented by the strain-hardening behavior in uniaxial tension. Details of these micromechanical analyses can be found in Li and Leung [6].

2.2. Use of slag particles

In order to achieve moderately high tensile strength (~5 MPa) and to improve the fiber dispersion, a method incorporating slag particles into cement particles is employed. A wealth of research [7,8] has been presented with regard to improving the rheological and mechanical properties using slag particles. Notably, it has been reported that slag can contribute to an increase in the flowability in a fresh state. In addition, the use of mineral admixtures (i.e., slag particles) is also desirable for economical and environmental considerations due to the lower cement requirement. This reduces the amount of carbon dioxide generated by the production of cement, while slag particles are a by-product material ordinarily produced from metallurgical processes. Thus, there is considerable environmental benefit from the use of slag particles.

From a micromechanical point of view, it is likely that the addition of slag particles will decrease the potential of high ductility, as the addition of slag in general results in an overall decrease in the water–binder ratio, leading to increases in J_{tip} and σ_{fc}. According to the micromechanical model for steady state cracking, which is essential for achieving strain-hardening behavior, a high J_{tip} value reduces the margin for the development of multiple cracking in terms of its effect on the toughness ratio (J_b'/J_{tip}). Therefore, the fiber bridging behavior was initially analyzed based on the micromechanical principle. The range of mixture proportion suitable for achieving desired ECC properties, represented by high ductile properties with tightly controlled multiple cracks, was then determined.

Although slag particles result in decreased potential for saturated multiple cracking, the use of slag is expected to provide benefits in terms of improving the fiber dispersion. It is well known that fiber dispersion is one of the key factors in achieving sufficient mechanical performance of fiber-reinforced cementitious materials. The expected enhancement of fiber dispersion originates from enhanced workability, attributed to the electrical double layer formed by the oxidized grain surface. Slag is a vitreous particle which has a polarity due to the broken Si–O bonds. The fresh

Table 1
Selected mix composition

Cement	Water	Sand	Slag	HRW [a]	HPMC [b]
1.0	0.60	0.8	0.25	0	0.001
1.0	0.48	0.8	0.25	0.02	0
1.0	0.35	0.8	0.25	0.03	0
1.0	0.60	0.8	0	0	0.001
1.0	0.48	0.8	0	0.02	0
1.0	0.35	0.8	0	0.03	0

All numbers are mass ratios of cement weight.
[a] High-range water-reducing admixture.
[b] Hydroxypropylmethyl-cellulose.

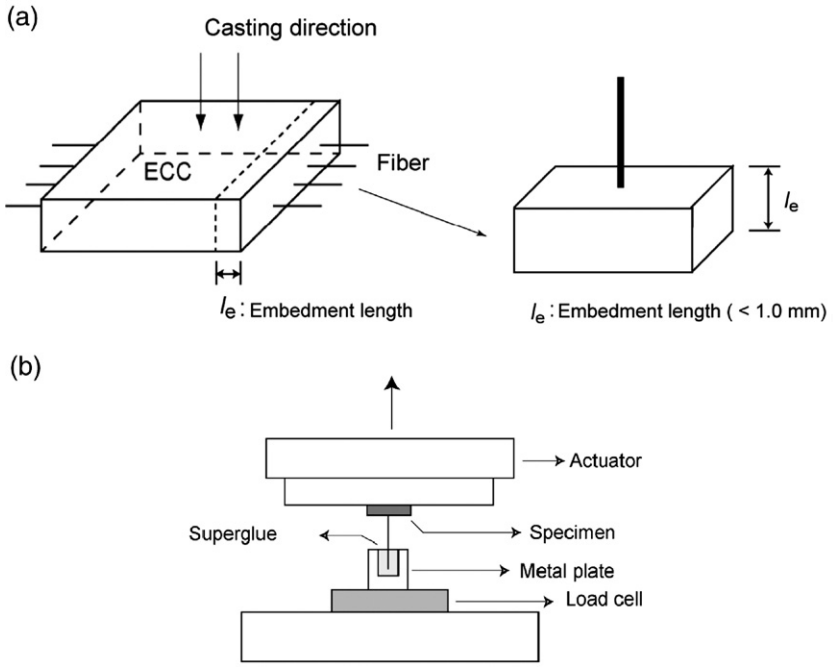

Fig. 2. Single fiber pullout test for (a) the specimen preparation and (b) the test setup.

behavior of Slag-ECC is expected to be positively influenced by the interactions between the cement particles and slag particles. It was found in a previous study [9] that vitreous slag particles can adsorb super-plasticizer molecules and form an electrical double layer on their surfaces, thus producing a dispersion effect in the paste. This provides a driving force to the mortar matrix flow, resulting in good fiber dispersion. The dispersion effect of slag particles should not be considered as a micro-filling effect, because the size of the slag particles is similar to that of cement particles. Other experimental results confirm that the dispersion effect is more effective in enhancing the fluidity of cement-based materials, and is related to the vitreous phase [10].

3. Experimental programs

3.1. Materials

ECC is essentially composed of a common mortar matrix and polymer fibers. In this study, a polyvinylalcohol (PVA) fiber

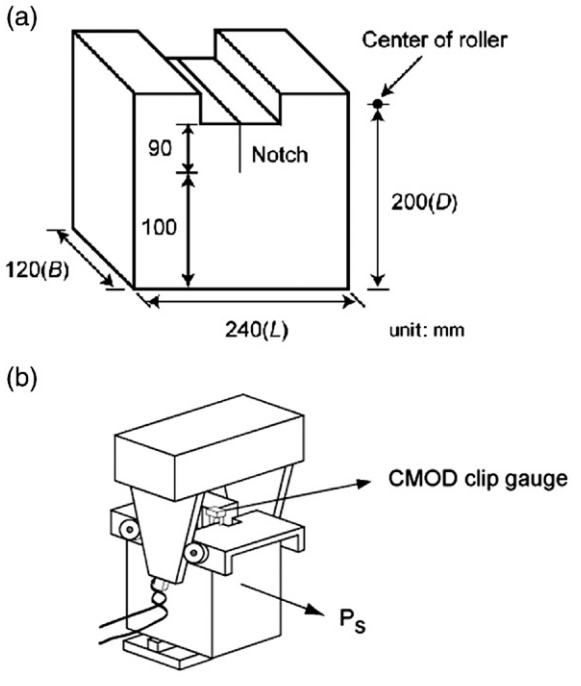

Fig. 3. Matrix fracture toughness test for (a) the specimen geometry and (b) the test setup.

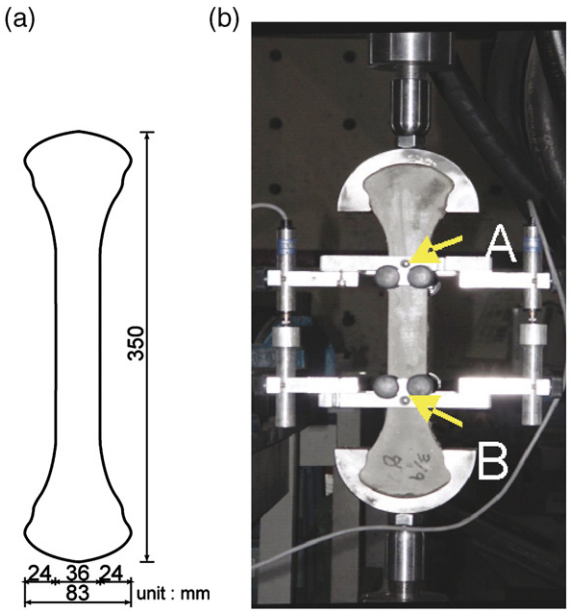

Fig. 4. Direct tensile test for (a) the specimen geometry and (b) the test setup.

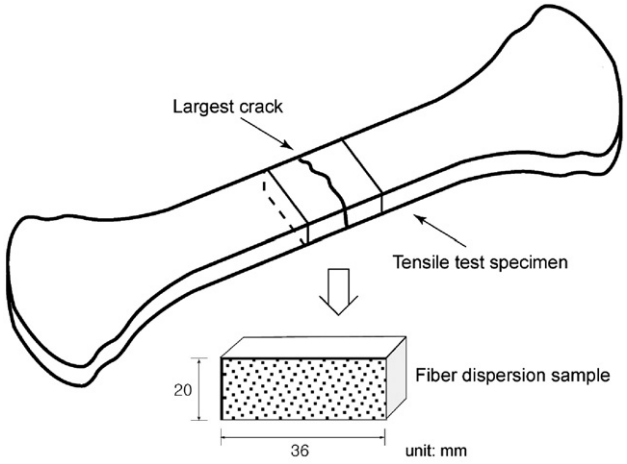

Fig. 5. Two samples obtained from one tensile specimen for the evaluation of fiber dispersion.

(Kuraray Co. Ltd., REC15, fiber length = 12 mm, Japan) was used as the reinforcing fiber. Type I ordinary Portland cement (C, Ssangyong Co., average particle diameter = 11.7 ± 4.8 μm, Korea), silica sand (S, Saehan Silica Co., average particle diameter = 130 ± 38 μm, Korea), and ground granulated blast furnace slag (Slag, Basic Materials Co., average particle diameter = 11 ± 3 μm, Korea) were used as the major ingredients in the matrix. Chemical admixtures comprised of a high-range water-reducing admixture (HRW, Atex Co., Korea) and hydroxypropylmethyl-cellulose (HPMC, Atex Co., Korea) were used to modify the fluid properties.

3.2. Tests for obtaining micromechanical properties

The appropriate mixture of ingredient (cement, sand, water, and chemicals) loading was determined from preliminary micromechanical analyses and mixing tests, as shown in Table 1. With the aim of attaining increased tensile strength and enhanced workability, 25% addition of slag particles (in terms of the mass fraction of cement particles) was selected based on the manufacturer's recommendations and preliminary mixing tests, resulting in water–binder ratios of 48%, 38%, and 28%.

3.2.1. Fiber pullout test

A single fiber pullout test was employed to measure the interfacial properties. Fig. 2(a) illustrates the specimen preparation and experimental setup. Ten specimens were cast together in a small Plexiglas mold. They were demolded at 2 days, followed by curing in water. The day prior to testing, the specimens were modified to the desired thickness, which corresponds with the fiber embedment length, l_e. The fiber embedment length was chosen to be nearly 1.0 mm in an effort to ensure full debonding. The pullout tests were conducted on an Instron machine with the specimen configuration shown in Fig. 2(b). A 10-N load cell was used to measure the pullout load of the fibers with a displacement rate of 0.2 mm/min. The displacement was measured as the actuator movement. The fiber-free length was kept at a maximum of 1 mm.

3.2.2. Matrix fracture test

A wedge-splitting test (WST) method was employed to test the mortar matrix fracture toughness. The dimensions and shape of the WST specimens are shown in Fig. 3(a). A 90-mm-long initial notch was made by inserting a 1-mm-thick steel plate inside the specimen during the casting process and subsequently removing the plate after 1 day. A groove was made in the upper part of the specimen for the placement of two load devices with roller bearings and to attach the displacement gages (CMOD clip gages). The principle of the WST is schematically presented in Fig. 3(b). The actuator of the testing machine was moved such that the wedge enters between the bearings, which results in a horizontal splitting force component. The load in the vertical direction and the crack mouth opening displacement (CMOD) as well as the location of the roller axis are monitored during testing. The efficacy of this method has already been demonstrated by the authors [11]. The loading speed was controlled at a constant rate (0.06 mm/min) of CMOD increment at the location of the roller axis. The specimen was monotonically loaded to the peak load.

3.3. Tests for demonstrating composite performances

To evaluate composite performances, SEM, direct tensile, and fiber dispersion tests were performed on selected specimens from four ECC mixes, which includes ECC mixes without slag (W/C of 60% and 48%) and Slag-ECC mixes (W/B of 48% and 38%).

3.3.1. SEM test

Secondary electron imaging was used for the compositional analysis. Evaluation of fractured surfaces provided morphological and bonding information related to the mechanical performance obtained from direct tensile tests. Specimens were analyzed after performing direct tensile tests using a Philips XL30 field emission gun (FEG) scanning electron microscope (SEM). A secondary electron (SE) detector, operated at 10.0 kV accelerating voltage, was chosen for the analysis of the fractured surfaces of direct tensile test specimens. To obtain an improved view of the fibers, some images were taken after tilting the samples by 75° with respect to the horizontal plane.

3.3.2. Direct tensile test

To verify the strain-hardening behavior of the cast ECC (both with and without slag) specimens, a series of direct tensile tests (three specimens for each ECC mix) were performed using an Instron 8506 load frame. The specimens were loaded with a constant cross head speed (0.2 mm/min), and the loading force and elongation were measured. Two linear variable differential transducers (LVDTs) attached to both sides of the center of the tensile specimen with a gage length of 150 mm in order to monitor the elongation. The gage length refers to the distance between points A and B, as shown in Fig. 4(b). To avoid fractures outside the measurement area, both ends of the specimens were made with a dog-bone shape. In addition to the tensile stress–strain curves, the ultimate tensile strength was measured, as was the ultimate tensile strain. Fig. 4 shows the specimen geometry and the test setup.

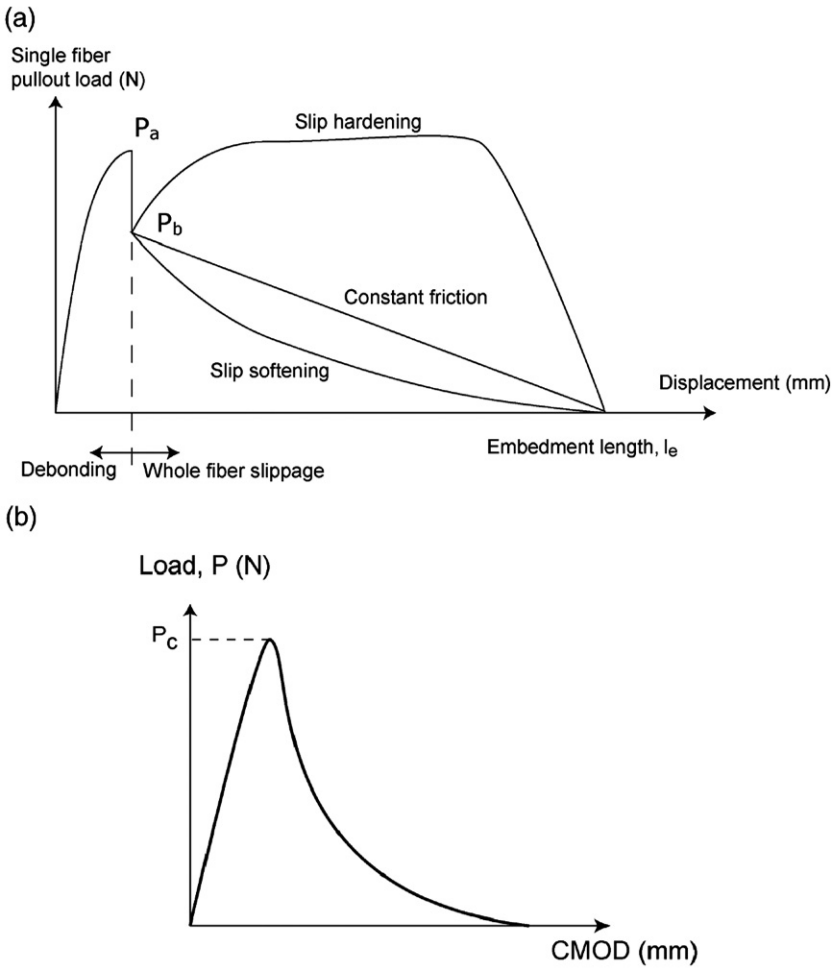

Fig. 6. Typical curves obtained from (a) a single fiber pullout test and (b) a mortar matrix fracture test.

3.3.3. Fiber dispersion test

A fluorescence technique was employed to evaluate the fiber dispersion performance of the ECC. For each ECC mix, a total of four samples were prepared with two fractured tensile specimens, which exhibited typical tensile performance. From one tensile specimen, as shown in Fig. 5, two samples with a height of 20 mm and a width of 36 mm were cut out using a diamond saw in order to obtain cross-sections in close proximity to the largest crack. This is because the weakest structure is normally located around the largest crack. With polishing, the cross-section of the sample was observed through a fluorescence microscope (Olympus, BX51). Using mercury lamp illumination, a fluorescence image was captured with a CCD digital camera (Olympus, U-TV) through a green fluorescent protein (GFP) filter under 4× magnification. The cross-sectional image was converted to a binary image analyzed by the use of image analysis software. The fiber dispersion performance was then evaluated based on the resultant binary image.

4. Results and discussion

4.1. Fiber pullout and matrix fracture tests

The general profile of a single fiber pullout curve is illustrated in Fig. 6(a). After debonding, the pullout curve exhibits slip hardening or slip softening depending on the fiber type, fiber/

Table 2
Test results (matrix with slag particles)

Age (days)	W/B=48% (W/C=60%)			W/B=38% (W/C=48%)			W/B=28% (W/C=35%)		
	τ_0 (MPa)	G_d (J/m^2)	J_{tip} (J/m^2)	τ_0 (MPa)	G_d (J/m^2)	J_{tip} (J/m^2)	τ_0 (MPa)	G_d (J/m^2)	J_{tip} (J/m^2)
7	1.39	1.77	2.02	1.42	1.79	3.28	1.47	1.81	6.43
14	1.43	1.83	2.79	1.50	1.87	4.63	1.54	1.87	8.92
28	1.65	1.88	3.23	1.85	1.83	5.42	1.94	1.86	10.04

Table 3
Test results (matrix without slag particles)

Age (days)	W/C=60%			W/C=48%			W/C=35%		
	τ_0 (MPa)	G_d (J/m^2)	J_{tip} (J/m^2)	τ_0 (MPa)	G_d (J/m^2)	J_{tip} (J/m^2)	τ_0 (MPa)	G_d (J/m^2)	J_{tip} (J/m^2)
7	1.30	1.80	1.68	1.40	1.92	2.85	1.49	1.80	5.49
14	1.36	1.81	2.35	1.49	1.84	3.81	1.53	1.84	7.26
28	1.62	1.82	2.67	1.82	1.85	4.53	1.90	1.70	8.59

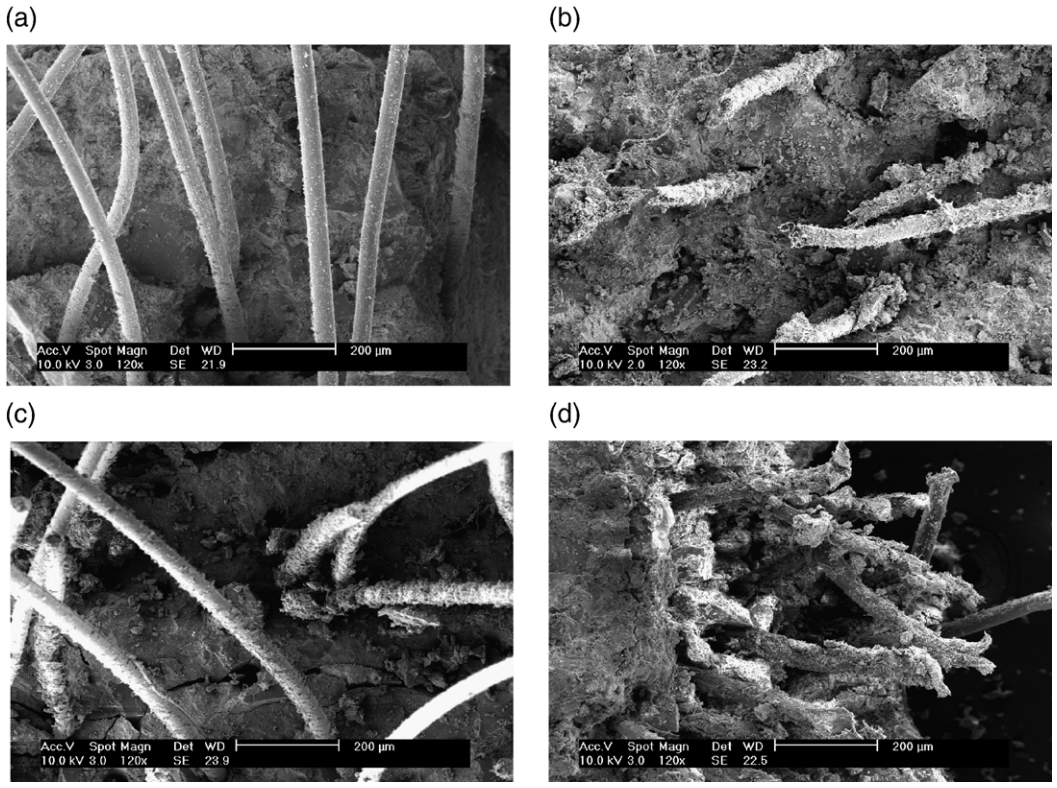

Fig. 7. SEM image taken from the fractured surface for (a) W/C=60% (without slag) mix; (b) W/C=48% (without slag); (c) W/B=48% (with slag); and (d) W/B=38% (with slag).

matrix bond strength, and specimen age. Based on this curve, the chemical debonding energy value G_d, is calculated from the P_a to P_b difference, as shown in Eq. (4).

$$G_d = \frac{2(P_a - P_b)^2}{\pi^2 E_f d_f^3} \quad (4)$$

where E_f is the Young's modulus of the fiber; P_a is the peak load during the debonding process; P_b is the peak load during the pullout process; and d_f is the fiber diameter [12]. From the P_b value, the frictional bond strength τ_0 at the onset of fiber slippage is calculated as follows:

$$\tau_o = \frac{P_b}{\pi d_f l_e} \quad (5)$$

A typical load–CMOD curve is shown in Fig. 6(b), from which the critical CMOD ($CMOD_c$) and critical peak load P_c are obtained. The fracture toughness K_{Ic} (=K_m) and the elastic modulus of the matrix E_c were calculated from the load–CMOD curves. Details of the empirical calculations can be found in a study by Murakami and Zhao [13,14]. Finally, J_{tip} was calculated using Eq. (2).

Tables 2 and 3 display the results obtained from the tests. Test results show that the properties tend to increase with decreasing water–cement ratio (W/C). As noted from these tables, there is no significant difference in G_d, independent of the addition of slag particles. This is attributed to the PVA fiber, a hydrophilic fiber, showing a strong chemical bond with the fresh cement matrix, of which G_d is principally determined by the chemical structures developed between the fiber surface and cement matrix. These chemical structures were not altered by the water content, and thus the chemical bond is independent of the matrix W/B [12]. In contrast, the addition of slag particles results in a slight increase (within 10%) of τ_0 at the same W/C. This is due to the decreased porosity in the interfacial zone with a decrease of W/B. This can lead to an increase of the fiber–matrix contact surface, resulting in a higher frictional bond.

This increase in fiber/matrix frictional bond strength with a decrease of W/B was verified with SEM image observations. The water–binder ratio, the porosity of the composite, the fiber morphology, and the matrix compaction play key roles in the resultant fiber–matrix interfacial bond in fiber–cement-based materials [15,16]. As shown in Tables 2 and 3, the frictional bond strength tends to increase with decreasing water–cement ratio. Also, the addition of slag particles yielded an increase in the frictional bond strength at the corresponding W/C. As explained earlier in this section, this is due to decreased porosity in the interfacial zone with a decrease of W/B, which was verified via SEM tests. The results for ECC (W/C=60%, W/C=48%) and Slag-ECC (W/B=48%, W/B=38%) are depicted in Fig. 7. Fig. 7(a) shows that the comparatively smooth surface of fibers predominantly results in fiber pullout. In contrast, Fig. 7(b) shows some fracture-ended filaments, indicating higher interfacial bonding with decreasing water–cement ratio. Comparing Fig. 7(a) with Fig. 7(c), the fiber surfaces in Slag-ECC have more attached matrix material compared to ECC without slag. This is because the former has higher frictional bonding with decreasing water–binder ratio. Higher

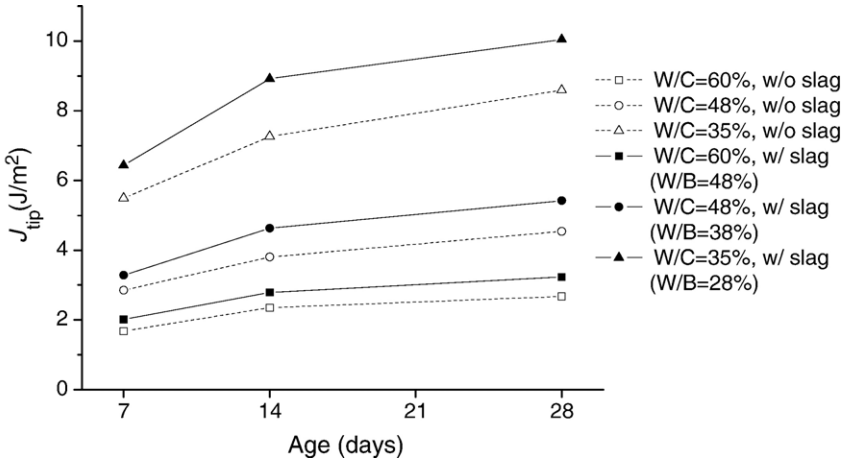

Fig. 8. Crack tip toughness J_{tip} as a function of the matrix age for the effects of W/C and the addition of slag particles.

frictional bonding may be detrimental to achieving sufficient multiple cracking and robust strain-hardening behavior. It should be noted, however, that Slag-ECC with W/B=48% has a smoother surface than that of the W/C=48% ECC, as shown in Fig. 7(b) and (c). This indicates that the Slag-ECC mix has comparatively low frictional bonding at the same water–binder ratio.

The effects of the W/C and the addition of slag particles on J_{tip} are illustrated in Fig. 8 as a function of the age of the matrix. The results indicate that the J_{tip} value increases with the addition of slag particles at an identical W/C. This is primarily due to the enhanced matrix strength caused by the presence of slag particles. Slag particles are most commonly activated by the hydration product of Portland cement, where calcium hydroxide formed during hydration is the principal activator. Slag hydration products lead to decreased porosity in the matrix, resulting in enhanced matrix strength and toughness. Higher matrix toughness may be detrimental to achieving desired mechanical properties, as it reduces the margin to develop multiple cracking in terms of toughness ratio. However, it should be noted that at an identical W/B ratio, the mix designed with slag particles exhibits lower J_{tip}, compared to the J_{tip} value of the mix without slag. This is almost certainly due to the retarded cementitious reactions of the slag, which consume part of the calcium hydroxide formed during the earlier stages of hydration. This indicates that the use of slag particles should be helpful for achieving strain-hardening behavior, as a lower J_{tip} value provides better opportunities for multiple cracking in the composite.

4.2. Fiber bridging analysis

To obtain the toughness ratio (J_b'/J_{tip}), a fiber bridging analysis was performed on composites reinforced with 2% PVA fibers in a volume fraction based on the micromechanical principle. The toughness ratios calculated from these analyses are displayed in Fig. 9. As shown in Fig. 9, all mixes sufficiently meet the steady state cracking requirement; specifically, $J_b'/J_{tip}=1$. However, from an experimental correlation between the intensity of multiple crack saturation and the toughness ratio of the composite, Kanda and Li estimated that a toughness ratio value equal to 3 is necessary to achieve saturated multiple cracking [17]. Based on their investigation, it was estimated that mixes of 35% W/C both with and without slag particles are not appropriate for obtaining

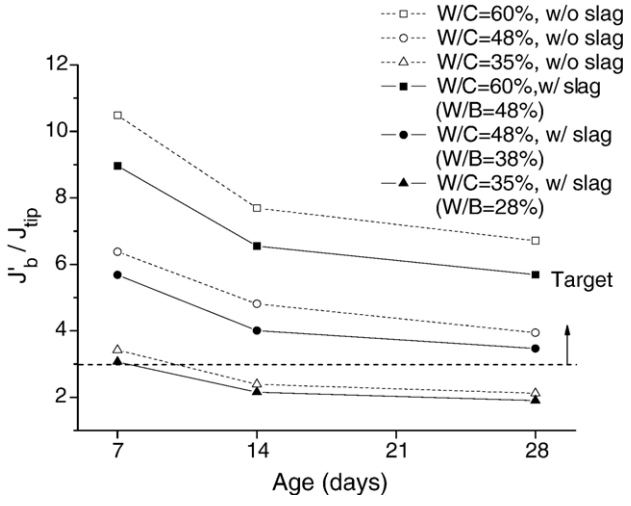

Fig. 9. The toughness ratio as a function of the composite age for the effects of W/C and the addition of slag particles.

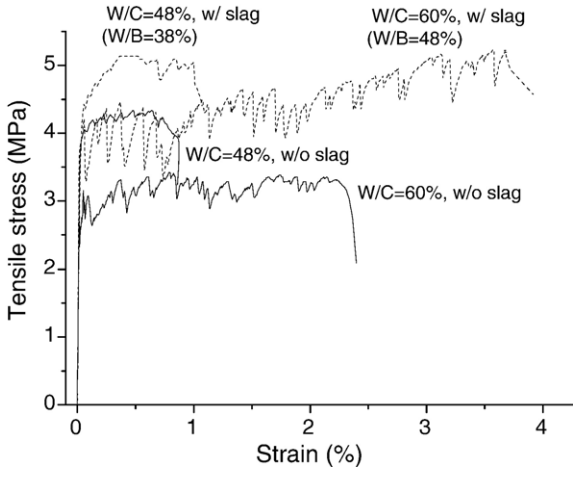

Fig. 10. Typical stress vs. strain curves in uniaxial tension.

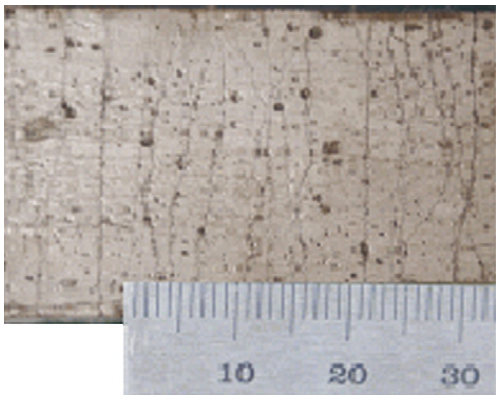

Fig. 11. Multiple cracking of specimen (W/C=60% with slag).

saturated multiple cracking. In addition, observations in the present set of experiments suggest that the mixes of 35% W/C are scarcely workable with the use of an ordinary mixing system. In terms of the toughness ratio and workability, a W/C ratio higher than 35% is preferable in practice.

4.3. Optimized range of Slag-ECC mixture proportion

An appropriate range of Slag-ECC mixture ingredient loading was determined from extensive micromechanical analyses and experiments, as detailed in the previous sections. It was found that a water–cement ratio ranging from 48% to 60% with a sand–cement ratio (S/C) ratio of 80% would be appropriate to achieve satisfactory mortar matrix properties. To demonstrate the optimal W/C ratio, direct tensile tests were performed on composites with W/Cs of 48% and 60% (both with and without slag) at 28 days, respectively. The direct tensile test is considered to be the most accurate and effective method to confirm the strain-hardening behavior of a composite, as quasi-brittle FRC can potentially show apparent strain-hardening behavior under flexural loading, depending on the specimen geometry. The test results in terms of typical stress–strain curves are presented in Section 4.4.

4.4. Uniaxial tension performance

Direct tensile tests were performed on cast specimens of the ECC in order to confirm the ductile strain-hardening performance of the hardened composite. Typical stress–strain curves from each ECC mix are presented in Fig. 10 for comparison. All specimens exhibit apparent multiple cracking patterns accompanying pseudo strain-hardening behavior with strain capacities ranging from 1.0% to nearly 3.6%. This ductility remains much higher than that in normal concrete and conventional FRC composites. However, the mixes of W/C=48% show relatively lower strain capacity when compared to the ductility of the mixes of W/C=60%. It appears that the toughness ratio of the mixes with a W/C=48% is very close to the required ratio ($J_b'/J_{tip}=3$, Fig. 9), and thus a sufficient margin for obtaining saturated multiple cracking cannot be provided. However, at an identical water–binder ratio, Slag-ECC with W/B=48% exhibits a much higher strain capacity relative to the composite with W/C=48%. Note that Slag-ECC with W/B=48% has an approximately 40% higher toughness ratio compared to that of the W/C=48% mix, as shown in Fig. 9, thus indicating that the W/B=48% mix has a sufficient margin for obtaining saturated multiple cracking, as previously described in Section 4.2.

The addition of slag particles (W/B=48% mix with slag) leads to higher tensile strain capacity (3.6±0.3%) accompanied by greater composite strength (5.2±0.2 MPa in tensile strength) than those of the composite without slag (strain capacity of 2.4±0.2% and tensile strength of 3.4±0.3 MPa). High strength of Slag-ECC is basically due to the enhanced matrix strength caused by the reduced water–binder ratio. High strain capacity of Slag-ECC, however, was not expected since this composite exhibited a smaller margin of toughness ratio relative to the composite without slag. Therefore, we hypothesized that the superior strain capacity of Slag-ECC is attributable to the presence of slag particles, since the particles should contribute to improved fiber dispersion performance, which is associated with enhanced workability. This trend was verified by performing fiber dispersion tests, as detailed in Section 4.5. The comparison of strain capacity suggests that, within the limited slag dosage employed in the present experiments, the contribution of slag particles to the workability outweighs the side-effect of decreased potential for saturated multiple cracking. Fig. 11 shows saturated multiple cracking in one of the specimens (W/C=60% mix with slag). Shortly after initial cracking, the crack width grows rapidly

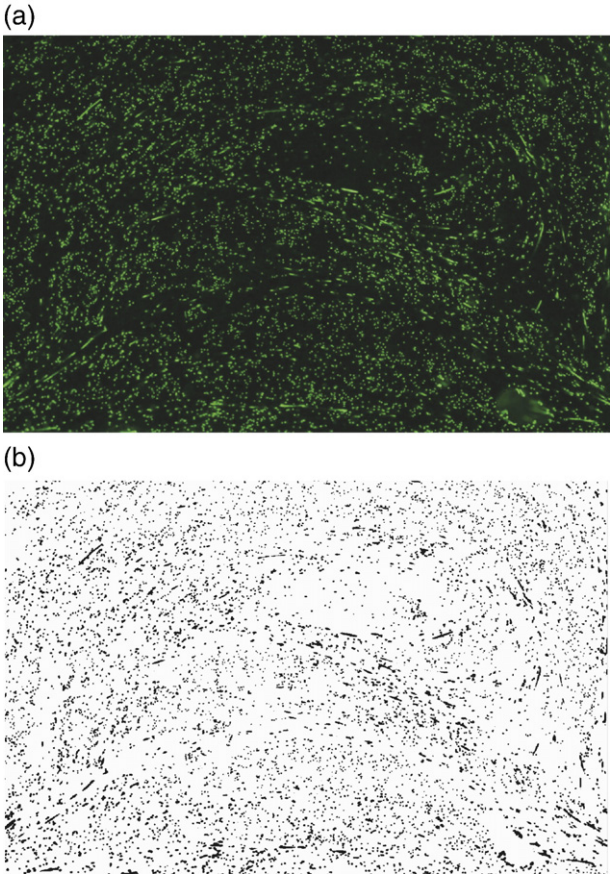

Fig. 12. Processed images for (a) cross-sectional fluorescence image and (b) binary image.

with an increase of strain, and then stabilizes at about 60 μm while additional micro-cracks further develop.

4.5. Fiber dispersion performance

The superior strain capacities of Slag-ECC compared to ECC are most likely due to the contribution of the slag particles to improved fiber dispersion. To test this hypothesis, we performed a fiber dispersion test by analyzing a binary image (Fig. 12(b)) converted from the cross-sectional fluorescence image (Fig. 12(a)). In this test, we assumed that the characteristics of the fiber orientation were constant regardless of the mixture proportion. To quantify the fiber dispersion performance, we developed an image processing program. In the process, coordinate data of all the fibers were automatically obtained, and the cross-sectional binary image was then divided into a large number of equal squares, which is equivalent to the total number of fibers in the section. The fiber dispersion performance was quantitatively evaluated by Eqs. (6) and (7), which calculate the coefficient of variation and distribution, respectively. The coefficient of variation $\phi(x)$ was calculated during the image processing based on the number of fibers in a square, x_i, and the number of squares, n (Eq. (6)). The distribution coefficient α was then simply calculated as given in Eq. (7) [18].

$$\phi(x) = \sqrt{\frac{\Sigma(x_i - 1)^2}{n}} \tag{6}$$

$$\alpha = \exp[-\phi(x)] \tag{7}$$

The calculated distribution coefficients are plotted in Fig. 13. Slag-ECC exhibits higher values than ECC without slag, demonstrating that Slag-ECC has more homogeneously distributed fibers in the composite. This results in approximately 50% higher strain capacity relative to ECC without slag. This supports the hypothesis that slag particles provide a driving force to mortar matrix flow and well-dispersed fibers, thereby leading to a more ductile composite. The evaluation method of fiber dispersion in the composite is thus an important technique for developing new ECCs, details of which will be presented in a follow-up paper.

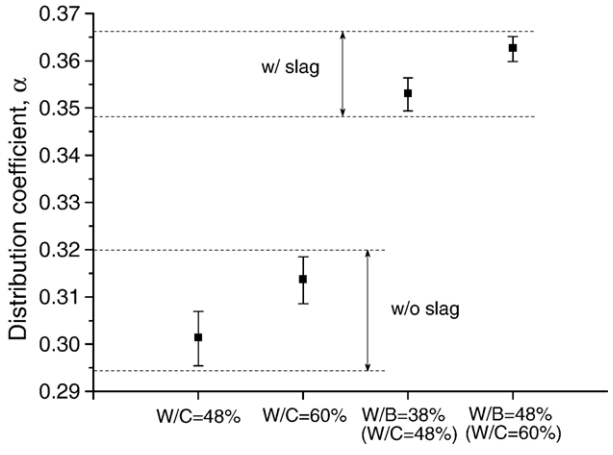

Fig. 13. Distribution coefficient plotted with the ECC mix, for which two cross-sections near the fractured surface of the tensile specimen are tested.

5. Conclusions

An ECC mixture proportion with satisfactory tensile behavior was developed by employing slag particles with the use of a micromechanical analysis. In the material development process, a series of tests were preformed to obtain the fiber–matrix interfacial properties and matrix fracture properties required for analyzing the fiber bridging behavior, followed by demonstration tests including direct tensile, SEM, and fiber dispersion tests. The following conclusions can be drawn from the experimental and analytical results:

(1) An optimized range of the Slag-ECC mixture proportion was obtained. This was determined based on the micromechanical principle. A micromechanical analysis was initially performed to select the appropriate water–binder ratio based on the results from single fiber pullout tests and matrix fracture tests. The basic matrix proportion range was then determined based on fiber bridging analysis results and workability considerations.

(2) Both ductility (3.6±0.3% for the tensile strain capacity) and tensile strength (5.2±0.2 MPa for the tensile strength) of the Slag-ECC were measured to be significantly higher than these values for the ECC without slag. The ECC mix designed with slag particles exhibited a lower J_{tip} value at an identical W/B ratio, compared to that of the mix without slag. Therefore, Slag-ECC demonstrated a higher toughness ratio when compared to ECC without slag at an identical W/B ratio. This indicates that the use of slag particles should be helpful for achieving strain-hardening behavior, as the higher toughness ratio is associated with a higher likelihood of multiple cracking in the composite.

(3) Although the toughness ratio decreases with the addition of slag particles at an identical W/C (60%), the tensile strain capacity of Slag-ECC is approximately 50% higher than that of ECC without slag. This is likely attributable to the contribution of slag particles to improvement of the fiber dispersion performance. Improved fiber dispersion appears to originate from enhanced workability, which is attributed to an electrical double layer formed by the oxidized slag surface.

(4) To demonstrate the hypothesis that slag particles provide a driving force for high fiber dispersion and consequent high strain capacity, we performed a fiber dispersion test by analyzing a binary image converted from a cross-sectional fluorescence image. Test results indicate that Slag-ECC exhibits higher distribution coefficients than ECC without slag, demonstrating that Slag-ECC has more homogeneously distributed fibers in the composite relative to ECC without slag. This result suggests that, within the limited slag dosage employed in the present study, the contribution of slag particles to the workability

outweighs the detrimental side-effect (higher J_{tip}) of decreased potential for saturated multiple cracking.

Acknowledgments

This study has been a research project supported by the Korea Ministry of Construction and Transportation through the Korea Advanced Institute Science and Technology (A06-04). The authors wish to express their gratitude for the financial support that made this study possible.

References

[1] V.C. Li, S. Wang, C. Wu, Tensile strain-hardening behavior of polyvinyl alcohol-engineered cementitious composite (PVA-ECC), ACI Materials Journal 98 (6) (2001) 483–492.
[2] V.C. Li, Reflections on the research and development of ECC, Proceedings of the JCI Int'l Workshop on Ductile Fiber Reinforced Cementitious Composites Application and Evaluation (DRFCC' 2002), Takayama, Japan, , Oct. 2002, pp. 1–21.
[3] Y.Y. Kim, H.-J. Kong, V.C. Li, Design of engineered cementitious composite suitable for wet-mixture shotcreting, ACI Materials Journal 100 (6) (2003) 511–518.
[4] Y. Shi, I. Matsui, N. Feng, Effect of compound mineral powders on workability and rheological property of HPC, Cement and Concrete Research 32 (1) (2002) 71–78.
[5] N. Feng, Y. Shi, T. Hao, Influence of ultra-fine powder on the fluidity and strength of cement paste, Advances in Cement Research 12 (3) (2000) 89–95.
[6] V.C. Li, C.K.Y. Leung, Steady state and multiple cracking of short random fiber composites, Journal of Engineering Mechanics, ASCE 188 (11) (1992) 2246–2264.
[7] C.K. Park, M.H. Noh, T.H. Park, Rheological properties of cementitious materials containing mineral admixtures, Cement and Concrete Research 35 (5) (2005) 842–849.
[8] M. Penpolcharoen, Utilization of secondary lead slag as construction material, Cement and Concrete Research 35 (6) (2005) 1050–1055.
[9] J. Hill, J.H. Sharp, The mineralogy and microstructure of three composite cements with high replacement levels, Cement and Concrete Composites 24 (2) (2002) 191–199.
[10] Y. Shi, I. Matsui, Y. Guo, A study on the effect of fine mineral powders with distinct vitreous contents on the fluidity and rheological properties of concrete, Cement and Concrete Research 34 (8) (2004) 1381–1387.
[11] J.K. Kim, Y.Y. Kim, Fatigue crack growth of high strength concrete in wedge splitting test, Cement and Concrete Research 29 (5) (1999) 705–712.
[12] T. Kanda, V.C. Li, Interface property and apparent strength of high-strength hydrophilic fiber in cement matrix, ASCE Journal of Materials in Civil Engineering 10 (1) (1998) 5–13.
[13] Y. Murakami, et al., Stress Intensity Factors Handbook, Pergamon Press, New York, 1987.
[14] G. Zhao, H. Jiao, S. Xu, Study on fracture behavior with wedge splitting test method, Fracture Processes in Concrete, Rock and Ceramics, E&F.N. Spon, London, 1991, pp. 789–798.
[15] R.S.P. Coutts, Fiber–matrix interface in air-cured wood-pulp fiber–cement composites, Journal of Materials Science Letters 6 (2) (1987) 140–142.
[16] H. Savastano Jr., P.G. Warden, R.S.P. Coutts, Microstructure and mechanical properties of waste fiber–cement composites, Cement and Concrete Composites 27 (5) (2005) 583–592.
[17] T. Kanda, V.C. Li, A new micromechanics design theory for pseudo strain hardening cementitious composite, ASCE Journal of Engineering Mechanics 125 (4) (1999) 373–381.
[18] S. Torigoe, T. Horikoshi, A. Ogawa, T. Saito, T. Hamada, Study on evaluation method for PVA fiber distribution in engineered cementitious composite, Journal of Advanced Concrete Technology 1 (3) (2003) 265–268.